Research Article

Yusong Liu, Fanbin Meng*, Jichuan Huang, Lijuan Ni, Yingdong Shen, and Liyan Zhang

Polyphenylene sulfide-coated wrench composites by nanopinning effect

https://doi.org/10.1515/ntrev-2021-0014
received January 12, 2021; accepted March 16, 2021

Abstract: When using a wrench, the nut is easily damaged due to improper operation or impact. Although coating a polymer layer on the surface of the wrench can effectively solve the above problem, the layer is easy to be deboned due to the lack of adhesion between the polymer and the surface of the wrench. Herein, we implemented an anodizing treatment strategy on the surface of the wrench to obtain a porous oxide film. Interestingly, during the anodization process, micro-nanopores with a specific diameter can be obtained by adjusting the voltage, temperature, and electrolyte concentration. Furthermore, the ammonium fluoride/ethylene glycol electrolyte was used to etch the formed large hole to form the large hole sleeve small hole structure. In order to inject polyphenylene sulfide (PPS) molecules into multiscale holes to form a pinning effect, we also used nano molding technology to inject PPS into the metal surface. The results showed that the adhesion between PPS and the wrench was greatly improved compared with the commonly used dip coating method.

Keywords: anodization, micro-nanopores, nano molding technology, pinning effect

*** Corresponding author: Fanbin Meng,** Key Laboratory of Advanced Technologies of Materials (Ministry of Education), School of Materials Science and Engineering, Southwest Jiaotong University, Chengdu 610031, China, e-mail: mengfanbin_wing@126.com
Yusong Liu: School of Mechanical and Electrical Engineering, Nanjing University of Aeronautics and Astronautics, Nanjing 213300, China; Chengdu Aircraft Industrial (Group) Co., Ltd, Chengdu, China
Jichuan Huang: Chengdu Aircraft Industrial (Group) Co., Ltd, Chengdu, China; School of Electronics and Information, Northwest University of Technology, Xian 710114, China
Lijuan Ni, Yingdong Shen: Chengdu Aircraft Industrial (Group) Co., Ltd, Chengdu, China
Liyan Zhang: School of Mechanical and Electrical Engineering, Nanjing University of Aeronautics and Astronautics, Nanjing 213300, China

1 Introduction

Wrenches play an important role in life. They are not only tools that can tighten bolts, nuts, and screws, but also have the function of a measuring device that can display the tightening torque or send a specific signal when a preset torque is reached [1,2]. However, when using a wrench, the nut is easily damaged due to improper operation or impact. In addition, in long-term use, the wrench inevitably produces wear and corrosion, which greatly reduces its performance [3–5]. Therefore, in order to avoid the wear of the workpiece and extend its service life, it is necessary to modify it.

The formation of polymer coatings on metal surfaces as metal–resin composites with potential industrial application, including decorative electrodes [6], corrosion protection [7,8], microelectronics [9,10], electronic products [11], aerospace equipment accessories and materials [12,13], *etc*. At present, the preparation methods of metal–resin composite materials mainly include lamination [14], laser welding [15], friction seam welding [16], friction stir welding [17], ultrasonic welding [18], and nano molding technology (NMT) [19]. Although coating a layer of polymer on the surface of the wrench can effectively extend its service life, the layer is easy to be deboned due to the lack of adhesion between the polymer and the surface of the wrench.

In order to solve the problem of adhesion between the polymer and the substrate surface, many researchers have made considerable efforts [20–24]. The traditional dipping method mainly refers to the introduction of reactive small molecules or functional groups on the metal surface after relevant treatment, such as irradiation crosslinking [25], and the interaction of molecules and atoms between the interface and resin to achieve bonding. However, the bond between the metal surface and the resin is easily affected by the environment, such as temperature, humidity, and so on. As we all know, due to the widespread application of anodic aluminum oxide film, the subsequent NMT to prepare new lightweight metal–resin materials has been developed [26,27]. The main

principle of NMT is that the amine compound reacts with a specific resin and generates heat to promote the flow of the resin in the nanopore; the resin embedded in the metal surface forms an anchor after curing between the two phases, thereby greatly improving the interface bonding strength. The NMT can not only effectively simplify the production process, reduce production cost, and improve product quality, but also extend product life and make product structures more diverse. It shows broad development prospects in industrial production and daily life applications.

Porous alumina is generally produced on Al using an electrochemical method called anodization. Anodization or anodic oxidation is a well-known process for growing oxide on valve metals such as Ti, Al, and Nb [28–31]. The anodic oxidation of metals can lead to the development of self-ordering pores [32,33]. It is carried out either by controlling the anodization voltage or by applying constant current to the substrate metal. The choice of anodizing method is very important because it directly affects the pore size of the porous anodized aluminum; it affects the size of nanostructures that are fabricated in porous anodic aluminum [34]. And key process parameters are electrolyte, composition, and temperature as well as the applied voltage or current. For example, Stepniowski *et al.* prepared anodized aluminum oxide in 0.3 M oxalic acid with a voltage range of 20–60 V and a temperature range of 35–50°C. They found that the best arrangement of nanopores was anodized aluminum formed at a voltage of 40–50 V. In addition, the distance between the aperture and the aperture increased linearly with the voltage [35]. Metal–resin composite materials can be obtained by anodic oxidation, most of them are concentrated in aluminum [36] or aluminum alloy as the main metal, while other metals (such as iron, nickel, or alloys containing iron and nickel) get rarely practical application [37–42].

Therefore, this article mainly initiated research on the application of metal wrench tools containing iron and nickel. The controllable micro and nano holes were prepared on the metal surface by anodic oxidation method, and then the assembly tools with high adhesive strength and protective performance were prepared by injecting the polyphenylene sulfide (PPS) resin material onto the metal surface using NMT [43,44]. Compared with the original bonding method of metal and synthetic resin combining with adhesive [45] at room temperature or under heating, the problem of poor adhesion between the two materials and poor acid and alkali resistance of adhesive is avoided. A certain amount of micro-nanopores was prepared by anodizing the metal, and then using NMT to inject PPS resin material on the metal surface. During the anodic oxidation process, we studied the effects of voltage, temperature, and electrolyte concentration on micro-nanopores. In the NMT, we studied the bond strength between different modified PPS and the metal of the wrench tool after injection molding and the torque on the wrench tool. A new type of wrench tool of lightweight metal material that can be used daily is obtained.

2 Methods

2.1 Materials

The wrench tool used for anodizing comes from Chengdu Hong Wei Future Mechanical and Electrical Company. The pure PPS used in injection molding and PPS resin modified with different glass fiber content are all from Da Han Chemical Company. Ammonium fluoride, ethylene glycol, hydrazine hydrate, acetone, and ethanol are all purchased from Ke Long Chemical Company. The reagents used in the experiment are all analytical reagents (AR), without further purification.

2.2 Anodizing the surface of the wrench tool

Before anodic oxidation, ethanol and acetone were used to ultrasonically remove oil stains on the surface of the wrench tool and dried at 60°C air flow. Then in a glycol electrolyte containing 0.1 mol/L NH_4F and a certain amount of deionized water, the wrench tool is used as the anode, and the graphite sheet is used as the cathode. Anodizing is performed at 20°C under a constant voltage of 20 V and stirring at different times. After anodizing, the wrench tool was placed in an oven at 60°C for 20 min to dry.

2.3 PPS plastic sleeve wrench tool preparation

Before injecting the wrench tool, dry the PPS and the PPS is modified with different glass fibers at 140°C for 6 h, then put the wrench tool into the pre-designed mold and perform injection at 280°C. The injection pressure is 48 MPa and the pressure is kept for 8 s. Take out the wrench tool after injection and perform mechanical performance tests such as hardness, pull-off, and torque.

2.4 Characterization

Scanning electron microscopy (SEM) was used to study the surface morphology and energy-dispersive X-ray spectroscopy (EDS) energy spectrum analysis of the anodized and unanodized wrench tools before and after the tool. The scanning was performed under high vacuum and 20.0 kV. An X-ray diffractometer (XRD) was used to characterize the structural changes before and after anodization of the wrench tool. The XRD used a copper target, the operating voltage was 60.0 kV, the current was 100.0 mA, and the scanning range was 10–60°. 200HRS-150 digital cloth hardness tester was used to measure the hardness of polystyrene resin plastic sleeve on the spanner tool surface. Hy-0580 electronic pull-off tester was used to test the adhesive force of the spanner tool. In addition, SGXJ torque tester was used to test the torque of the spanner tool after injection.

3 Results

Before anodizing the wrench, the distribution of elements on the surface of the wrench was tested. The result is shown in Figure 1. From Figure 1, it can be obtained that the elements on the surface of the wrench without anodization are mainly Cr and Ni, and a small amount of Fe and C. At the same time, the non-anodized spanner section after cutting was scanned by EDS to obtain the mapping spectrum of the element distribution of the spanner section in Figure 2. From Figure 2, the main elements under the plating layer of the spanner are Fe and a small amount of Al.

The wrench tool was added with ethylene glycol, 0.9 mL of deionized water, and 0.1 mol/L NH_4F solution as electrolyte, and the tool was anodized for 10–90 min at a voltage of 20 V. The morphology of the anodized samples after treatment was characterized, and the SEM diagram of the wrench surface at different times was obtained in Figure 3. Figure 3b shows that when dealing with 10 min, 20 V can form part of the holes in the surface of wrench. Figure 3c–j are SEM images with increased processing time. It can be seen that as time increases, the surface of the wrench hole gradually increases and becomes more structured, and the shallow holes on the surface become irregular, reaching the best state at 60 min. At the same time, in order to explore whether the surface elements changed after anodic oxidation, EDS surface scanning was carried out for the sample processed at

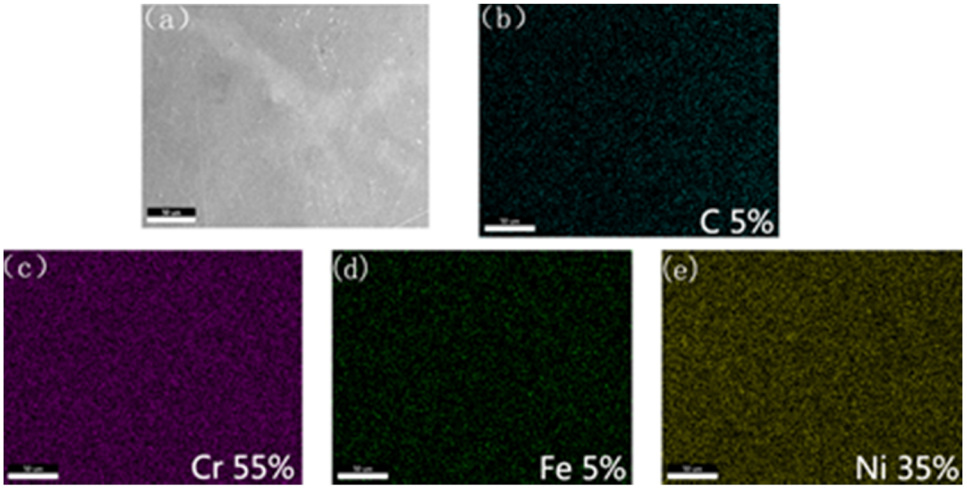

Figure 1: EDS sweep spectrum of wrench surface. (a) SEM image of wrench surface, (b) C 5%, (c) Cr 55%, (d) Fe 5%, and (e) Ni 35%.

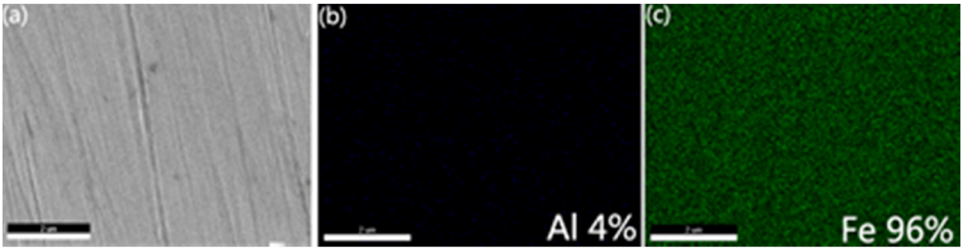

Figure 2: EDS spectrum of wrench section. (a) SEM image of wrench cross section, (b) Al 4%, and (c) Fe 96%.

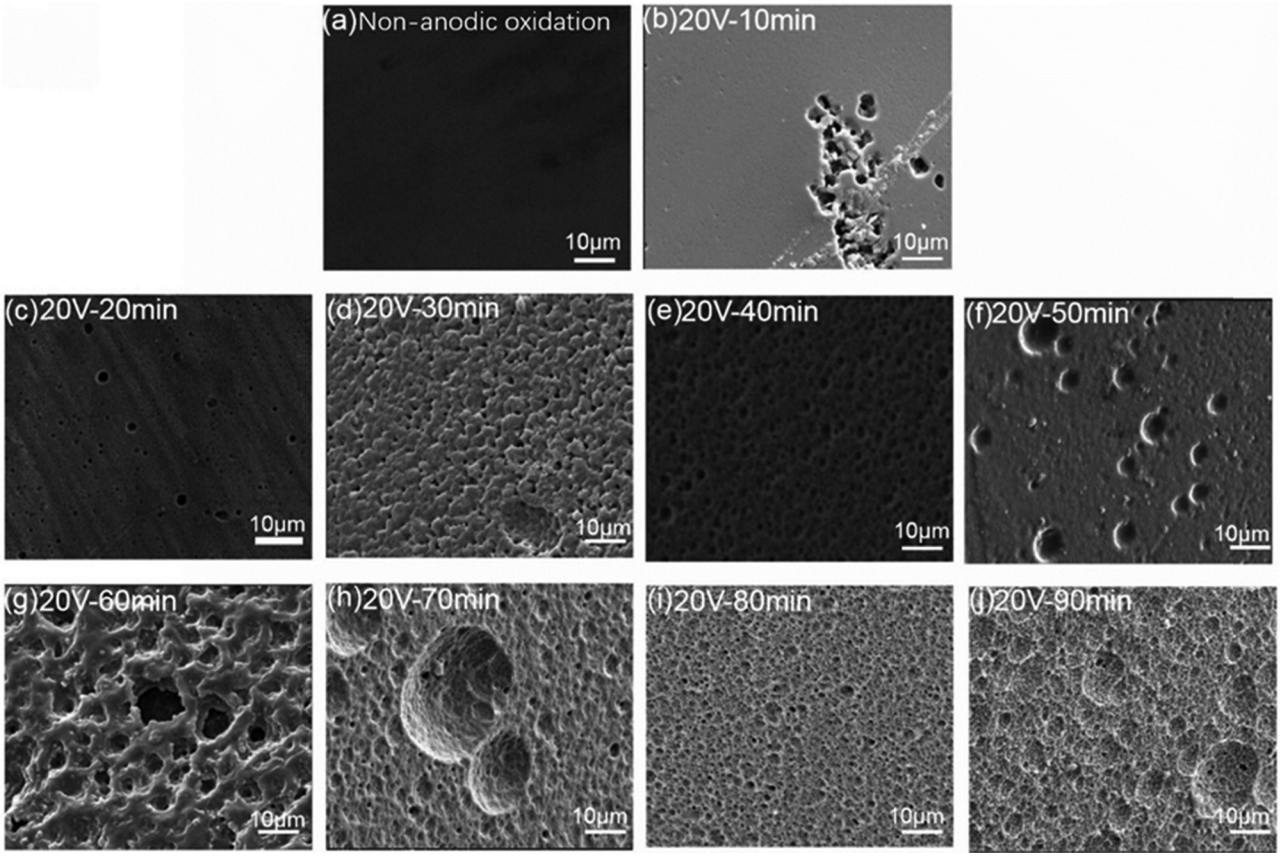

Figure 3: SEM images of the surface before and after different times were treated under 20 V: (a) Non-anodic oxidation, (b) 10 min, (c) 20 min, (d) 30 min, (e) 40 min, (f) 50 min, (g) 60 min, (h) 70 min, (i) 80 min, and (j) 90 min.

20 V for 60 min. Figure 4 shows the mapping spectrum of the surface of the spanner after anodic oxidation. Figure 4 shows that the elements on the surface of the spanner after anodic oxidation are mainly Ni, Fe, Al, O, and Co. Generally, in an anodizing process, the formed porous anodized film will first appear as a barrier layer. As the anodic oxidation time increases, the electrons in the electrolyte will transfer to the anode, breakdown the

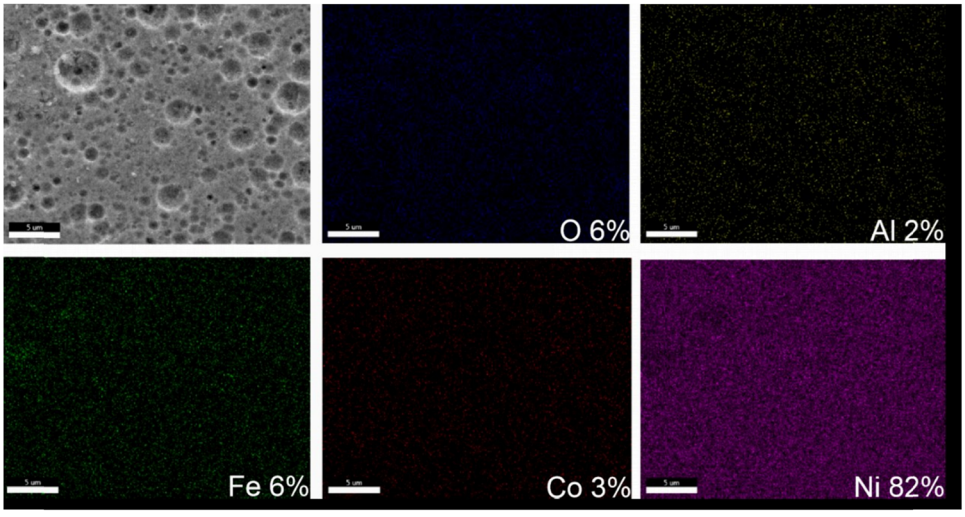

Figure 4: EDS diagram of the surface of the lower wrench treated with 20 V for 60 min.

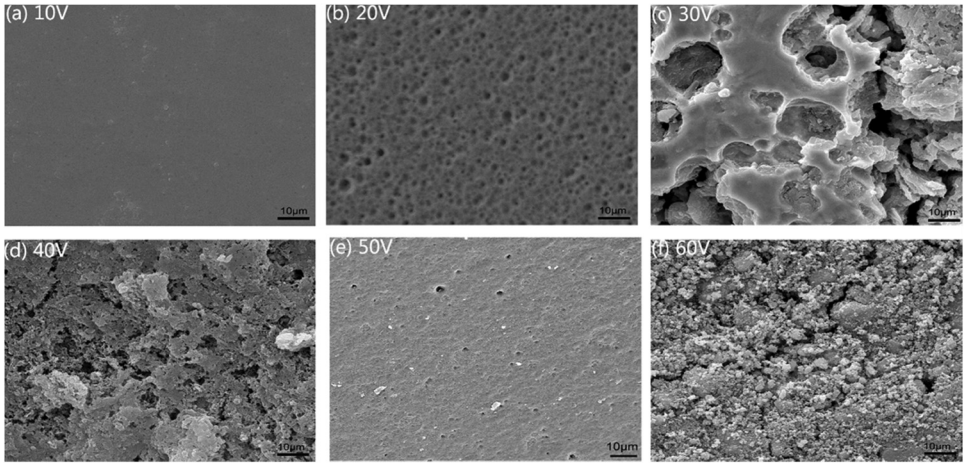

Figure 5: SEM images of spanner surface treated with different voltages for 40 min: (a) 10 V, (b) 20 V, (c) 30 V, (d) 40 V, (e) 50 V, and (f) 60 V.

barrier layer and oxide film on the metal surface, and generate some bubbles. However, after a certain period of time, the migration of anions and cations in the electrolyte is hindered, resulting in a decrease in oxidation efficiency. In addition, metal elements participating in anodization on the metal surface are blocked by other metal elements, thereby slowing down the anodization reaction speed. Therefore, if the reaction time is too long, the micro-nanopores on the alloy surface will decrease.

It is well known that the applied voltage has a great influence on the pore structure [46,47]. From Figure 3d, more holes can be found. In order to explore the best preparation conditions of the wrench on the hole surface, the wrench surface was anodized within 40 min under different voltages, and SEM images of the wrench surface under different voltage topologies were obtained, as shown in Figure 5a–f. From Figure 5a, the surface treatment after 40 min under 10 V does not show obvious holes, but after treatment under 20 V, clear and neat pores can be obtained. It can be seen from Figure 5c–f that as the voltage increases, the holes and cracks on the surface decrease, which shows that the best effect can be obtained under the condition of 20 V. When the voltage is low, gas will begin to precipitate at the barrier layer, so the porous structure will continue to be produced. However, when the voltage continues to increase, the barrier layer and the oxide film are broken down, and at the same time new oxide films are continuously formed and seal the first porous film, which will reduce the porous structure or even destroy the porous oxide film that is initially formed.

Figure 6 shows the surface morphology of the alloy surface obtained by anodizing the surface of the alloy for 60 min after changing the electrolyte concentration at 20°C. It can be seen from Figure 6a and b that as the concentration of ammonium fluoride in the electrolyte increases, the micropores on the alloy surface gradually become uniform and regular. However, when the concentration of ammonium fluoride in the electrolyte reaches 0.15 mol/L (Figure 6c) or higher, the opposite phenomenon occurs, with fewer pores on the surface and not particularly regular. Especially in Figure 6d, when the concentration reaches 0.2 mol/L, most of the pores on the surface disappear after anodization, and only some micro-nanopores appear in some positions. This is because during the anodic oxidation process, when the electrolyte concentration is low, it will react with the surface of the wrench, initially forming a small amount of relatively

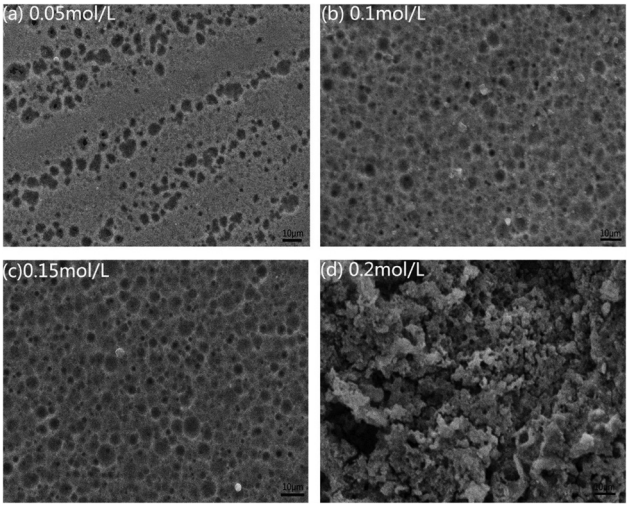

Figure 6: SEM image of the surface of anodized alloy with different concentrations of ammonium fluoride at 20°C: (a) 0.05 mol/L, (b) 0.10 mol/L, (c) 0.15 mol/L, and (d) 0.20 mol/L.

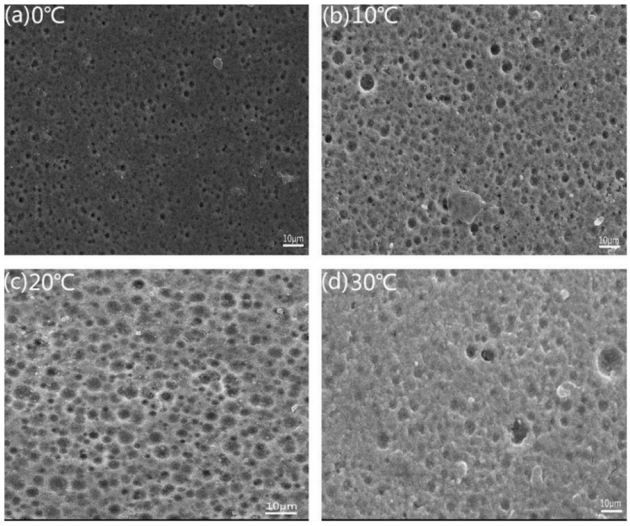

Figure 7: SEM spectra of spanner surface after anodic oxidation at different temperatures: (a) 0°C, (b) 10°C, (c) 20°C, and (d) 30°C.

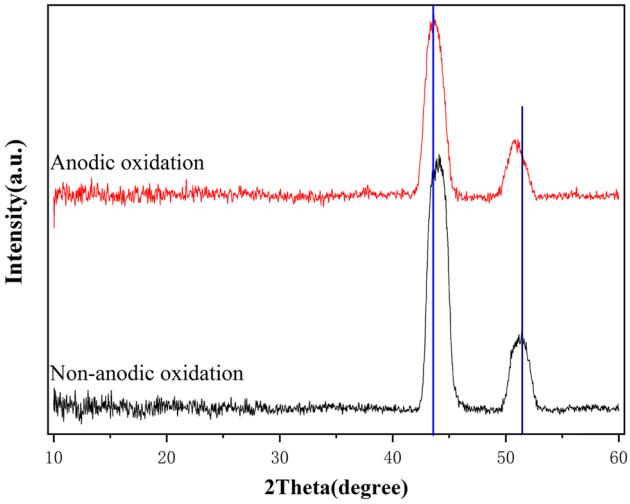

Figure 8: XRD pattern of spanner surface before and after anodic oxidation.

dispersed and small depth of micro-nano pores; but when the electrolyte concentration further increases, it will continue to interact with micro-nanopores. This reaction causes the total depth of the micro-pores to gradually increase and form partially connected pores, which results in a decrease in the number of pores but an increase in the average depth of the micro-nano pores.

In addition, the SEM image of Figure 7 is obtained by anodic oxidation of the alloy surface at different temperatures for 60 min. It can be clearly seen from the SEM images that with the gradual increase of temperature, the change of the micro-pores on the alloy surface becomes more obvious. Similarly, as the temperature increases, the number and regularity of holes gradually increase. However, when the reaction temperature reaches 30°C, the micro/nanopores on the alloy surface are reduced and no longer have uniform regularity. As the temperature increases, the porous anodic aluminum oxide layer is driven by the stress caused by its thin-walled pores. The main reason is that as the current increases, O_2 bubbles will form a strong scour effect of bubbles on the porous-type anodic aluminum oxide layers [48,49].

Figure 8 shows the X-ray diffraction spectra of a wrench before and after surface anodic oxidation. From the XRD spectrum, we can know that there are obvious peaks at 44° and 51.6° before anodization, but the peak after anodization changes 1° to the left. The formulation of Bragg's law shows that the lattice parameters of the anodic oxide film change, which may be mixed with other metal peaks, or it may be an anodic oxidation reaction, which leads to changes in the lattice parameters of the film. From the EDS analysis, we can know that there are elements such as Fe, Co, and Al in the wrench. On one hand, their metal oxides can cause the lattice distortion of nickel; on the other hand, they can also interact with Ni to form compounds. All these factors will cause the diffraction peak of Ni in the XRD pattern to shift to the left after anodization [50–52].

Generally, in the nanoinjection molding process, due to the pressure and temperature loss in the process, the resin will rapidly cool and solidify on the metal surface, so it is difficult to ensure its continuous flow [53,54]. In addition, in the cooling process, the volume shrinkage caused by the difference in thermal expansion coefficient between metal and resin will largely destroy the bond between resin and metal, resulting in holes or even falling off at the interface between the two phases. In order to solve this problem, Taisei Plas creatively developed a metal surface nanometer process: T treatment, which uses T liquid to etch the metal surface to produce nanometer holes. T treatment is a unique process of Taisei Plas, and T solution is a general term of T treatment solution. It requires different formulations for different metals and processes, but the main components are amine-based water-soluble reagents, such as hydrazine hydrate and ethylenediamine. The amine-based reagent was selected because N element is a strong electronegative element, which can form coordination bonds with the metal surface and adsorption on the surface. During the injection process, the amine groups in the T solution can react with the resin on the metal surface. Because the reaction is exothermic, the fluidity of the resin can be

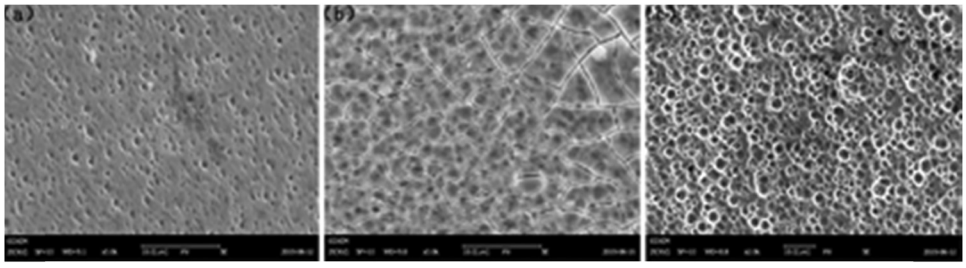

Figure 9: Surface morphology of spanner treated with T liquid for 30 min after anodic oxidation: (a) 20 V – 40 min, (b) 20 V – 50 min, and (c) 20 V – 60 min.

effectively maintained during the cooling process and the volume shrinkage of the resin can be prevented [19].

Figure 9 shows the surface morphology of T liquid (hydrazine hydrate) treated for 30 min after anodic oxidation at 20 V [12]. It can be seen from Figure 9a–c that the spanner surface after T liquid treatment has many uniform and orderly holes, and in Figure 9c, we can find that there are many smaller holes in many large holes.

Figure 10 shows the surface morphology of T liquid (hydrazine hydrate) treated for 60 min after anodic oxidation at 20 V. There are many uniform and structured pores on the surface of the wrench after T solution treatment. It can be seen from the comparison with Figure 9 that under the same anodizing condition, when the time after T solution treatment increases, the pores will increase. And in some areas, the holes will become larger, resulting in reduced structuring time. A large number of studies have shown that, in a certain range, the increase of the average area and average depth of metal micro-nanopores is beneficial to the anchor effect between metal and

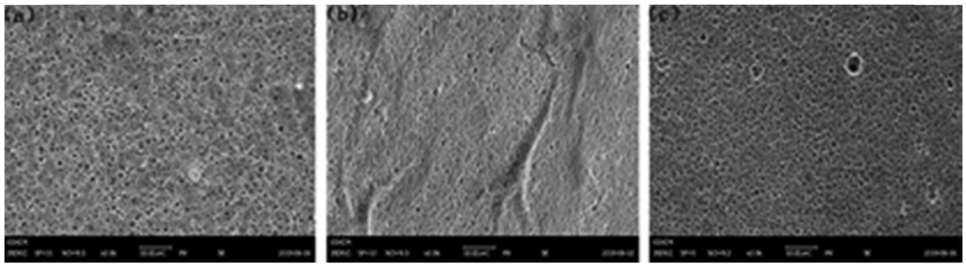

Figure 10: Surface morphology of spanner treated with T liquid for 60 min after anodic oxidation: (a) 20 V – 40 min, (b) 20 V – 50 min, and (c) 20 V – 60 min.

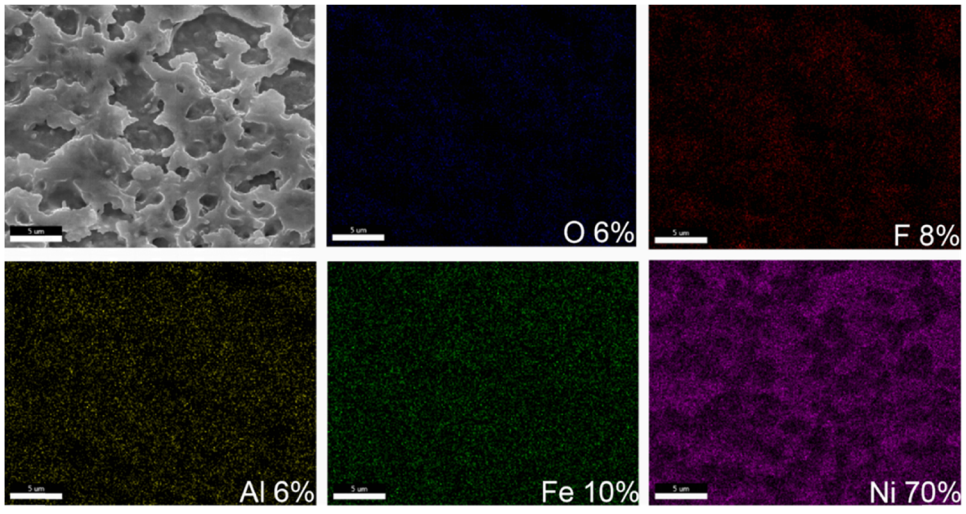

Figure 11: EDS diagram of the surface of the wrench treated with T liquid for 30 min after anodic oxidation.

plastic, which increases the bonding strength and surface adhesion of the products [55,56]. In addition, since hydrazine hydrate is a strong reducing agent, it can reduce metal oxides to metal elements [57,58]. Therefore, when the anodized metal substrate is treated with hydrazine hydrate, part of the oxide on the porous oxide film will be reduced to elemental metal and fall from the oxide film, which will cause new pores to be formed on the original anodized film.

Figure 11 shows the surface mapping of the wrench under T liquid treatment for 30 min after anodic oxidation. It can be seen from Figure 11 that after etching with hydrazine hydrate, the elements on the surface of the wrench include a small amount of oxygen, fluorine, aluminum, and iron and a large amount of nickel. By comparing the mapping spectrum after anodic oxidation and hydrazine hydrate treatment, it can be seen that the percentage of oxygen on the surface of both has not changed. However, when compared with Figure 9, it can be seen that the percentages of Fe and Al have increased, while the percentages of Ni have decreased.

The particle size statistical distribution of the small holes in the large holes on the surface morphology diagram prepared by T liquid treatment for 30 min is shown in Figure 12. According to the statistical results on the SEM picture, it is found that the pore size is distributed within 0–5 μm. In order to facilitate statistics, the particle size is divided into ten ranges. The percentage of the number of holes in each small range to the total number of holes is calculated to obtain the size distribution map on the right side of Figure 12. The weighted calculation results show that the average size of the pore diameter in the whole SEM diagram was 1.02 μm according to the particle size statistical distribution in Figure 12.

In order to inject PPS resin into the surface of the anodized wrench, we used the heads at both ends of the wrench tool as a template and designed the head of the wrench tool in Figure 13. Considering that the thickness of the plastic sleeve on the surface of the wrench tool is too thick to be used normally, when designing the injection mold diagram, the parameters of the mold are designed to inject 1 mm on the head of the wrench tool. PPS can ensure that the wrench tool after injection molding can still be used normally in daily life. And because it has excellent acid and alkali resistance,

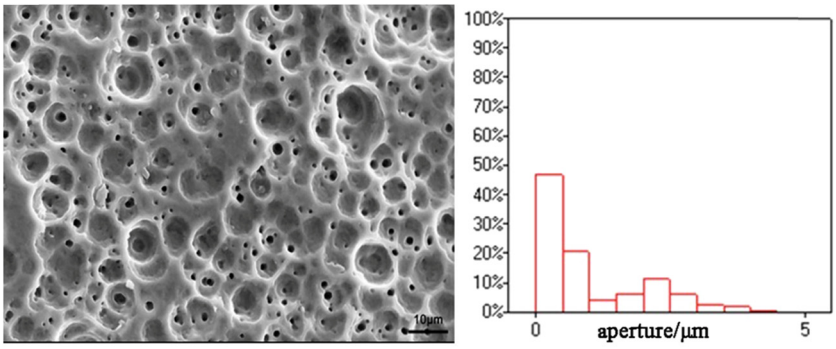

Figure 12: Histogram of pore size distribution after T liquid treatment for 30 min.

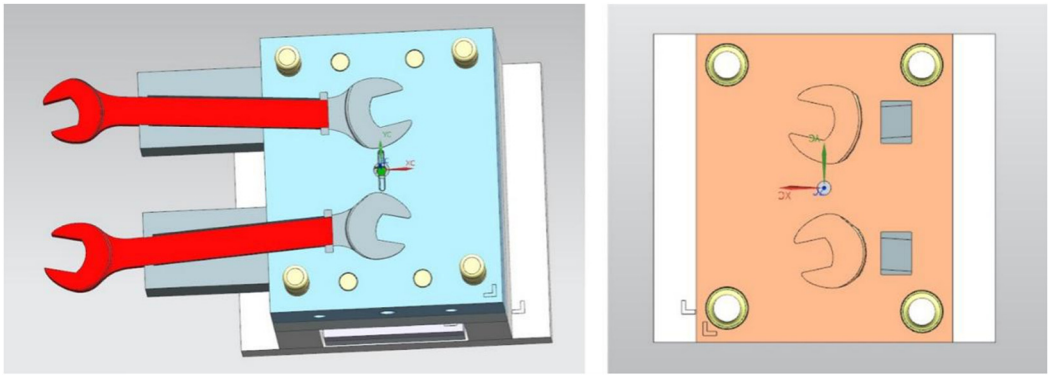

Figure 13: Wrench tool injection polymer plastic sleeve mold design drawing.

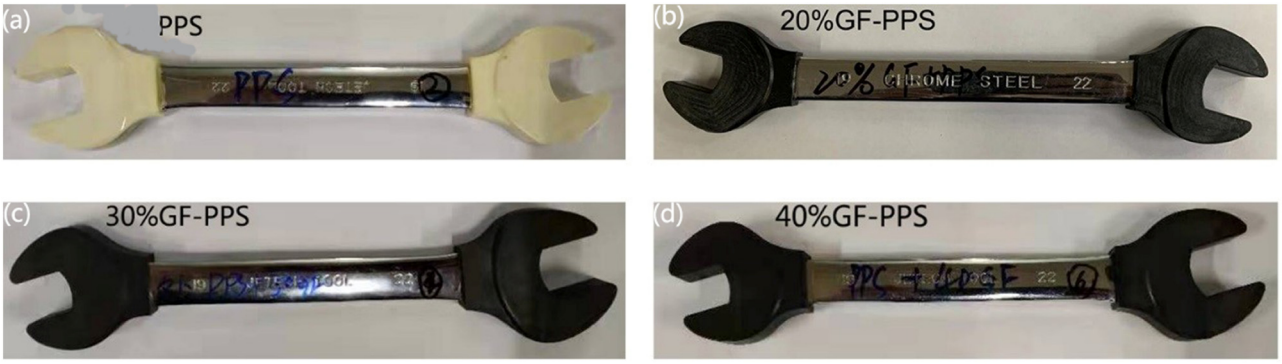

Figure 14: Digital photos of polymer sleeve obtained from different polymer injection molding of spanner head: (a) PPS, (b) 20% GF/PPS, (c) 30% GF/PPS, and (d) 40% GF/PPS.

it also improves the environmental resistance of the wrench [59].

After anodic oxidation is performed on the surface of the wrench tool, a layer of PPS resin injection molding material is coated on the surface of the wrench tool. It is recognized in the industry that the bonding strength between metal and plastic is not less than 80 MPa (or the drawing force is not less than 160 kgf), while the material must have a lower coefficient of thermal expansion and creep so that the bonding strength between metal and metal parts can withstand the influence of high and low temperature, humidity, and so on. Therefore, the relevant mechanical properties of the surface of the wrench tool were also tested (Figure 14).

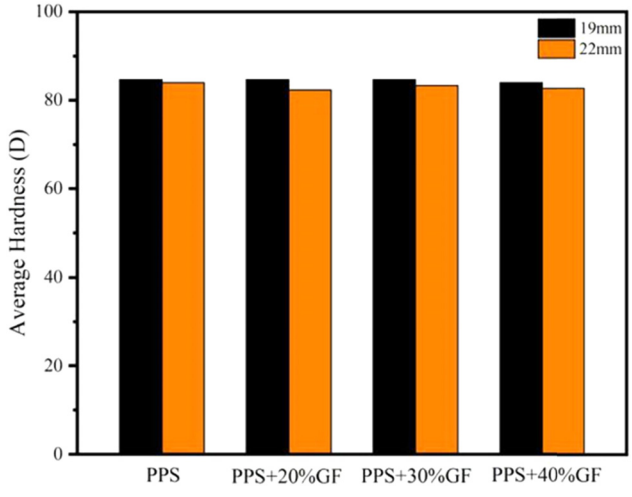

Figure 15: The hardness test results of polymer sleeve obtained from different polymer injection molding of spanner head.

Through the hardness test of a layer of PPS resin injected on the surface of the spanner, the results in Figure 15 are obtained. From Figure 15, we can get the injected polymer resin material, whether or not glass fiber is added, its hardness is about 84D. Because glass fiber is mainly added to increase impact or tensile properties, it usually does not increase the hardness of the material itself.

The pull-out test was performed on the surface of the wrench by injection molding PPS vulcanized plastic sleeve (Table 1). When the weight of 50 kg was applied for 3 min, it indicates that the plastic sleeve and the surface of the wrench have a good bonding force. The PPS resin melt enters the nanopores on the surface of the alloy substrate under high pressure, reacts with the "T treatment agent" remaining in the micro-nano pores, and releases heat during the reaction to prevent the front end of the melt from solidifying too fast to enter nanoscale holes. After the reaction is completed, the PPS resin structure produces an "anchor effect" and is fastened to the surface of the alloy substrate, thus making the joint

Table 1: Test results of pull-off experiment of PPS plastic sleeve on spanner tool surface

Sample name	Test position (mm)	Test result
PPS + 20% GF	19	Hang the weight of 50 kg for 3 min, the polymer plastic sleeve has no deformation and displacement
	22	Hang the weight of 50 kg for 3 min, the polymer plastic sleeve has no deformation and displacement

Table 2: Test results of polymer plastic sleeve on spanner tool surface

Sample name	Test position (mm)	Measured size (mm)	The torque (N/m)
PPS	22	18.42	40
PPS + 20% GF	22	18.43	45
PPS + 30% GF	22	18.44	47
PPS + 40% GF	22	18.39	48

have a high bonding force. The torque of pure PPS resin polymer sleeve is 40 N/m (Table 2), the torque of PPS resin with 20% glass fiber is 45 N/m, and the torque of PPS resin with 30 and 40% glass fiber is 47–48 N/m, but the plastic sleeve has some deformation.

4 Discussion

We conducted anodizing studies on wrench tools at different concentrations of ammonium fluoride/glycol electrolyte, different temperatures, different voltages, and different times. When the electrolyte concentration is 0.1 mol/L and the temperature is 20°C, the material exhibits the best performance. When the anodizing voltage is 20 V and the time is 60 min, the surface of the wrench tool can be controlled to obtain uniform and regular micro-nanopores.

The hardness of all wrenches after injection molding obtained through the pull test of the hardness tester is about 84D. In addition, under the weight of 50 kg, the PPS + 20% GF was pulled out for 3 min without removing the plastic sleeve from the wrench, indicating that there is a good bonding force between the resin and the surface of the wrench. The torque test shows that whether it is pure PPS or modified glass fiber, the torque is greater than 40 N/m. And the torque of 40% GF/PPS can reach 48 N/m, which is suitable for the normal applications of narrow pipelines.

Acknowledgments: The authors would like to thank the Analytical and Testing Center of Southwest Jiaotong University for supporting the relative measurements.

Funding information: This work was financially supported by the National Natural Science Foundation of China (NSFC, No.51903213), and the Science and Technology Planning Project of Sichuan Province (No. 2020YFH0053).

Author contributions: All authors have accepted responsibility for the entire content of this manuscript and approved its submission.

Conflict of interest: The authors state no conflict of interest.

References

[1] Ogushi K. The test evaluation of several digital torques wrenches by using a torque wrench tester. ACTA IMEKO. 2020;9(5):189–93.
[2] Gutierrez J, Nicholls JI, Libman WJ, Butson TJ. Accuracy of the implant torque wrench following time in clinical service. Int J Prosthodont. 1997;10(6):562–7.
[3] Jha AK, Manwatkar S, Sreekumar K. Hydrogen-induced intergranular stress corrosion cracking (HI-IGSCC) of 0.35C–3.5Ni–1.5Cr–0.5Mo steel fastener. Eng Fail Anal. 2010;17(4):777–86.
[4] Chidambaram D, Clayton CR, Halada GP. Interactions of the components of chromate conversion coating with the constituents of aluminum alloy AA2024-T3. J Electrochem Soc. 2004;151(3):B151–9.
[5] Sun Y, Li K, Gao B, Sun PY, Fu HY, Liu Z, et al. Study on microstructure and wear resistance of Zr-17Nb alloy irradiated by high current pulsed electron beam. Rev Adv Mater Sci. 2020;59(1):514–22.
[6] Mekhalif Z, Delhalle J, Lang P, Garnier F, Caudano R. Electropolymerization of bithiophene on aluminum surfaces modified by $CH_3(CH_2)9$-SH and ϕ-(CH_2)m-SH, m = 0 to 3.1999. J Electrochem Soc. 1999;146(8):2913–8.
[7] Jutta K, Erhart H, Hans JG. Intergranular corrosion of iron-phosphorus alloys in nitrate solutions. Corros Sci. 1981;21(3):227–38.
[8] Moloznik KL, Briant CL, Mcmahon CJ. The effect of grain boundary impurities on the stress corrosion cracking of a low alloy steel. Corros Houst Tx. 1979;35(7):331–2.
[9] Burroughes JH, Bradley DDC, Brown AR, Marks RN, Holmes AB. Erratum: light-emitting diodes based on conjugated polymers. Nature. 1990;348(6299):352.
[10] Gustafson GM, Svensson L. Ammonia emissions from pigs on deep litter beds and in a strip grazing system. J Sustain Agric. 2003;23(2):41–51.

[11] Hirahara H, Aisawa S, Mori K, Narita E, Oishi Y. Study of interfacial chemistry on direct curing adhesion between Ni–P plating and rubber using 1,3,5-triazine-2,4,6-trithiol monosodium salt. Surf Interface Anal. 2003;35(12):953–9.
[12] Kunio M, Hidetoshi H, Yoshiyuki O. Development of resin-molding-releasing metal mold surface using perfluoroalkyl group-containing polymer plating. J Chem Soc Jpn Chem Ind Chem. 2000;2000(4):281–9.
[13] Voigt K, Heubner C, Lammel C, Schneider M, Michaelis A. Facile fabrication of nanostructured alumina membranes. Microporous Mesoporous Mater. 2020;302:110207.
[14] Botelho EC, Silva RA, Pardini LC, Rezende MC. A review on the development and properties of continuous fiber/epoxy/aluminum hybrid composites for aircraft structures. Mater Res. 2006;9(3):247–56.
[15] Katayama S, Kawahito Y. Laser direct joining of metal and plastic. Scr Mater. 2008;59(12):1247–50.
[16] Liu FC, Liao J, Nakata K. Joining of metal to plastic using friction lap welding. Mater Des. 2014;54(54):236–44.
[17] Takamasa O, Kazuyoshi K, Masakatsu M. Friction stir lap welding of thermoplastic resins to 3003 aluminum alloy. J Jpn Inst Light Met. 2015;65(9):403–10.
[18] Konchakova N, Balle F, Barth FJ, Mueller R, Eifler D, Steinmann P. Finite element analysis of an inelastic interface in ultrasonic welded metal/fibre-reinforced polymer joints. Comput Mater Sci. 2011;50(1):184–90.
[19] Sasaki H, Kobayashi I, Sai S, Kobayashi I, Sai S, Omoto T, et al. Direct adhesion of nylon resin to stainless steel plates coated with triazine thiol polymer by electropolymerization during injection-molding. Kobunshi Rombun Shu. 1998;55(8):470–6.
[20] Zhu YJ, Ma JL, Wang GX, Song KX, Stock HR. Corrosion behaviour of multilayer CrN coatings deposited by hybrid HIPIMS after oxidation treatment. Nanotechnol Rev. 2020;9(1):596–609.
[21] Wang XF, Xu P, Han R, Ren J, Li LY, Han NX, et al. A review on the mechanical properties for thin film and block structure characterised by using nanoscratch test. Nanotechnol Rev. 2019;8(1):628–44.
[22] Lepicka M, Gradzka-Dahlke M. The initial evaluation of performance of hard anti-wear coatings deposited on metallic substrates: thickness, mechanical properties and adhesion measurements-a brief review. Rev Adv Mater Sci. 2019;58(1):50–65.
[23] Bahce E, Cakir N. Tribological investigation of multilayer CrN/CrCN/TaN films deposited by close field unbalanced magnetron sputtering. Rev Adv Mater Sci. 2019;58(1):271–9.
[24] Wu Q, Miao WS, Zhang YD, Gao HJ, Hui D. Mechanical properties of nanomaterials: a review. Nanotechnol Rev. 2020;9(1):259–73.
[25] Fumio Y. A novel technology of radiation crosslinking; modification of biodegradable polymer at paste-like condition by irradiation. Pielgniarka I Poozna. 2000;11(11):233–6.
[26] Andoh N. Technology for injection bonding of hard resin to al alloy [NMT] and, technology for injection bonding for hard resin to other metal [New NMT]. J Jpn Soc Mech Eng. 2007;110(1060):164–5.
[27] Ltd TPC. Bonding technology between metal and resin by injection molding (NMT) technical summary, product samples and the technical possibilities. J Soc Instrum Control Eng. 2015.
[28] Belwalkar A, Grasing E, Geertruyden WV, Huang Z, Misiolek WZ. Effect of processing parameters on pore structure and thickness of anodic aluminum oxide (AAO) tubular membranes. J Membr Sci. 2008;319(1–2):192–8.
[29] Skatkov L, Lyashok L, Gomozov V, Tokareva I, Bayrachniy B. Anodic formation of nanoporous crystalline niobium oxide. J Electrochem Sci Eng. 2014;4:2.
[30] Kocaba M, Rnek C, Curioni M, Cansever N. Nickel fluoride as a surface activation agent for electroless nickel coating of anodized AA1050 aluminum alloy. Surf Coat Technol. 2019;364:231–8.
[31] Zhang XH, Zhang Y, Tian BH, Jia YL, Liu Y, Song KX, et al. Cr effects on the electrical contact properties of the Al_2O_3-Cu/15W composites. Nanotechnol Rev. 2019;8(1):128–35.
[32] Vinogradov NA, Harlow G, Carlà F, Evertsson J, Rullik L, Linpé W, et al. The observation of pore growth and self-organization in anodic alumina by time resolved X-ray scattering. ACS Appl Nano Mater. 2018;1(3):1265–71.
[33] Larsson A, Abbondanza G, Weronica L, Linpe W, Carla F, Mousley P, et al. Electrochemical fabrication and characterization of palladium nanowires in nanoporous alumina templates. J Electrochem Soc. 2020;167(12):122514 (10pp).
[34] Nazemi A, Abolfazl S, Sadjadi S. Controlling the anodizing conditions in preparation of an nanoporous anodic aluminium oxide template. Mater Sci Pol. 2014;32(4):565–70.
[35] Stepniowski WJ, Nowak-Stepniowska A, Michalska-Domanska M, Norek M, Czujko T, Bojar Z. Fabrication and geometric characterization of highly-ordered hexagonally arranged arrays of nanoporous anodic alumina. Pol J Chem Technol. 2014;16(1):63–9.
[36] Andoh N. Nano molding technology: aluminum alloy and hard resin integration technology by injection molding. Seikei-Kakou. 2004;16(9):588–91.
[37] Shin HG, Kim HY, Kim BH. Nano molding technology for optical storage media with large-area nano-pattern. Key Eng. Mater. 2008;86:925–30.
[38] Norio S. Anodic oxidation of cobalt in neutral and basic solution. J Electrochem Soc. 1979;10(7):016.
[39] Barrett CA, Johnston JR, Sanders WA. Static and dynamic cyclic oxidation of 12 nickel-, cobalt-, and iron-base high-temperature alloys. Oxid Met. 1978;12(4):343–77.
[40] Jean-Jacques D, Vittorio DN, Olivier C. Nickel-iron alloy-based anodes for aluminium electrowinning cells: EP, US6562224 B2[P]; 2001.
[41] Ebersbach U, Schwabe K, Ritter K. On the kinetics of the anodic passivation of iron, cobalt and nickel. Electrochim Acta. 1967;12(8):927–38.
[42] Habazaki H, Shimizu K, Skeldon P, Thompson GE, Wood GC. The behaviour of iron during anodic oxidation of sputtering-deposited Al–Fe alloys. Corros Sci. 2001;43(7):1393–402.
[43] Schwirn K, Lee W, Hillebrand R, Steinhart M, Gösele U. Self-ordered anodic aluminum oxide formed by H_2SO_4 hard anodization. ACS Nano. 2008;2(2):302–10.
[44] Losic D, Lillo M, Losic D Jr. Porous alumina with shaped pore geometries and complex pore architectures fabricated by cyclic anodization. Small. 2009;5(12):1392–7.
[45] Kubota Y, Kuriyama O. Polyphenylenesulfide resin composition: US, US4395512 A[P]; 1983.

[46] Zakir O, Idouhli R, Elyaagoubi M, Khadiri M, Aityoub A, Koumya Y, et al. Fabrication of TiO_2 nanotube by electrochemical anodization: toward photocatalytic application. J Nanomater. 2020;2020(1):1–11.
[47] Jeong C, Lee J, Sheppard K, Choi CH. Air-impregnated nanoporous anodic aluminum oxide layers for enhancing the corrosion resistance of aluminum. Langmuir. 2015;31(40):11040–50.
[48] Li JG, Wei HY, Zhao K, Wang MF, Chen DC. Effect of anodizing temperature and organic acid addition on the structure and corrosion resistance of anodic aluminum oxide films. Thin Solid Films. 2020;713:138359.
[49] Aerts T, Dimogerontakis T, Graeve ID, Fransaer J, Terryn H. Influence of the anodizing temperature on the porosity and the mechanical properties of the porous anodic oxide film. Surf Coat Technol. 2007;201(16):7310–7.
[50] Chen S, Kang C, Wang J, Liu CS, Sun K. Synthesis of anodizing composite films containing superfine Al_2O_3 and PTFE particles on Al alloys. Appl Surf Sci. 2010;256(22):6518–25.
[51] Hotovy I, Huran J, Spiess L. Characterization of sputtered NiO films using XRD and AFM. J Mater Sci. 2004;39(7):2609–12.
[52] Rahman MK, Nemouchi F, Chevolleau T, Gergauda PK. Ni and Ti silicide oxidation for CMOS applications investigated by XRD, XPS and FPP. Mater Sci Semicon Proc. 2017;71:470–6.
[53] Saha B, Toh WQ, Liu E, Tor SB, Hardt D, Lee J. A review on the importance of surface coating of micro/nano-mold in micro/nano-molding processes. J Micromech Microeng. 2016;26(1):01300.
[54] Ding J, Qin ZY, Luo HT, Yang W, Wang YB, Huang ZX. Nano-silica modified phenolic resin film: manufacturing and properties. Nanotechnol Rev. 2020;9(1):209–18.
[55] Meiers JC, Jensen ME, Mayclin T. Effect of surface treatments on the bond strength of etched-metal resin-bonded retainers. J Prosthet Dent. 1985;53(2):185–90.
[56] Qu J. Adhesion and failure of polymer-metal interfaces in microelectronic packaging. New York: Springer; 2014.
[57] Hong RY, Li JH, Cao X, Zhang SZ, Di GQ, Li HZ, et al. On the $Fe_3O_4/Mn_{1x}Zn_xFe_2O_4$ core/shell magnetic nanoparticles. J Alloy Compd. 2009;480(480):947–53.
[58] Agusta MK, Kasai H. First principles investigations of hydrazine adsorption conformations on Ni(111) surface. Surf Sci. 2012;606(7–8):766–71.
[59] Um C, Jung D, Yu SY, Lee SS, Lee HW, Lee PC, et al. Study on physical properties of polyphenylene sulfide composites with variothermal mold temperatures. Polymer-Korea. 2020;44(6):798–803.